GLOBALLY AUTOMATED LUNAR MARE AND MELT DETECTION USING DEEP LEARNING. X.-L. Cui[1], M. Ding[1], S. Yan[2], Q. Deng[3], and M.-H. Zhu[1] [1]State Key Laboratory of Lunar and Planetary Sciences, Macau University of Science and Technology, Macau, China (miding@must.edu.mo), [2]Leeds School of Business, University of Colorado Boulder, USA, [3]School of Information Management & Engineering, Shanghai University of Finance and Economics, Shanghai, China.

Introduction: Lunar mare deposits cover ~ 16% of the lunar surface, which is mainly located in the nearside [1]. These mare basalts are clearly identifiable by their dark colors and smooth surfaces in the optical images. Surface mare deposits indicate local volcanic activities, which provide significant constraints for the global thermal evolution of the Moon [e.g., 2].

Impact melts, on the other hand, are generated by exogenic impact processes [e.g., 3], which record the bombardment history of the planet. Although the impact melt and mare basalt have strikingly different origins, distinguishing them has found to be difficult from optical image due to similar surface roughness and textures [4]. Specially, mare basalts are preferentially erupted in large impact basins with reduced crustal thickness [5], implying spatial co-existence of these two types of geologic units.

Due to this intrinsic similarity, identifying the two units altogether from remote sensing optical observations is potentially more feasible than distinguishing them from each other. For the Moon, *Nelson et al.* [6] provide a global mare boundary map by visually identifying boundaries in the LROC Wide Angle Camera (WAC) images and Clementine UVVIS color ratio mineral map. But there is not yet an impact melt database available for the global lunar surface.

In this work, we take the advantage of the existing mare boundary map [6] to train a convolutional neural network (CNN), based on LROC WAC images. The network is expected to learn the characteristics of mare basalts in the optical images, and thus has the potential to detect lunar geologic units with similar optical characteristics. Our trained network discovers more mare-like areas than the input mare basalts, which we infer to be mainly impact melts.

Data and Training: We use the global mosaic of LROC WAC images with a spatial resolution of 100 m per pixel [7] as input data. The global WAC mosaic is cropped to square images of 512×512 pixels. The lunar mare boundary map [6] is projected to the same equal-sized squares as the ground truth. We denote Class 1 to represent a basaltic pixel, while Class 0 represents a non-basaltic pixel. About 6,500 cropped WAC images with ground truth are combined, among which we select 80% to train the network and the rest are used to test the performance of our trained model.

We implement a customized UNET architecture [8] based on deep learning for this detection task. This network consists of two main paths: the first path extracts features from original images; and the following second path outputs the predictions with the same size as the original images from expanding the extracted features. After training, for each pixel the network yields a classification result from 0 to 1, which can be directly compared with the input ground-truth labels.

Our trained network has achieved a high pixel classification accuracy (the ratio of the number of correctly predicted pixels to all the pixels) of 96%, indicating that the network has learned the optical

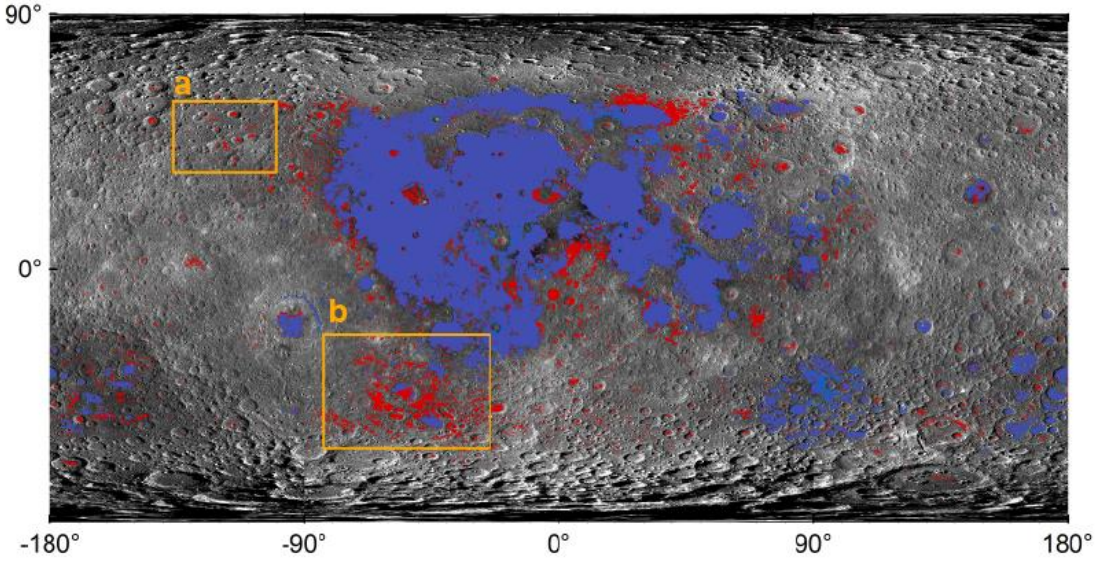

Fig. 1. Global map of detected mare and melt on the Moon. Blue color: Ground-truth mare basalt units from [6]; Red color: Our detected mare and melt units. Yellow boxes outline the locations of Fig. 2.

characteristics of lunar mare basalts as provided by [6]. Our *MIoU* (Mean Intersection over Union), defined as the ratio of the intersection and union of two sets of ground truth and prediction, is 78%, as we detect more mare-like areas than the input and the false positive detection greatly reduces the intersection of the ground truth and prediction sets. Nevertheless, the false positive detection is expected because we do not use mineral maps in the training. Furthermore, the false positives are actually newly discovered mare-like areas that turn out to be the major benefit of this study (see next section).

Results and Discussions: In total, we identify a mare-like surface area of about 6,910,000 km^2 (red areas in Fig. 1), corresponding to ~ 18% of the lunar surface area. Our detected area is visibly larger than the 16% provided by [6] (blue areas). This is mainly because we do not use mineral maps for training, and thus do not require mineral content characteristics of mare basalts to be satisfied. But the benefit of this method is that we detect new mare-like areas, which bear similarities in the optical characteristics with mare basalts. By visually inspecting the images with newly discovered mare-like areas, we find that the main feature for our detection is the surface smoothness and the boundaries are mostly placed between smooth and rough surfaces.

Comparing our newly discovered mare-like surface areas (red areas in Fig. 1) with the ground-truth mare basalt areas from [6] (blue areas) suggest that we have classified more areas surrounding the ground-truth areas to be mare-like. These new areas are likely mare basalts, which we will further confirm by zooming in the details of these areas.

More intriguing new detection are plenty of small areas scattered over the lunar highlands. Considering the different smoothness for lunar geologic features [9], the newly discovered smooth areas are most likely to be impact melts and cryptomare. Fig. 2a shows a detailed image of newly identified mare-like areas in a region to the west of Oceanus Procellarum (see Fig. 1). These identified mare-like areas are tightly associated with crater floors, implying that they are induced by impact processes. Although smooth areas in large craters are likely to be post-impact mare deposits (e.g., for the 218-km-diameter Landau crater indicated by a yellow circle), the areas within relatively small craters are most plausible to be impact melts because mare deposits are unlikely associated with small craters, in particular on farside highlands. We will compare with multispectral data to further study the composition and origin of these smooth features.

Fig. 2b shows newly discovered mare-like areas in the Schiller-Schickard region where the most extensive cryptomare on the Moon has been proposed [10]. In this region, cryptomare basalts facilitated by the ancient Schiller-Schickard basin (yellow circle) are super-imposed by subsequent Orientale ejecta deposits [e.g., 11]. But the existence of underlying ancient cryptomare basalts has been confirmed by dark-halo craters. Therefore, our technique also has the potential to detect cryptomare deposits due to their smooth surface.

Conclusions: This study combines the existing mare basalt map for the Moon and the modern deep learning technique to automatically detect mare-like geologic units with smooth surfaces. Our trained network is able to detect new mare-like areas that potentially correspond to impact melts and cryptomare deposits. We will compare with multispectral data to further confirm their composition and origin. Our study provides a viable way to train a neural network to automatize planetary geologic feature detection, which may be applied to other planets and for other remote sensing datasets.

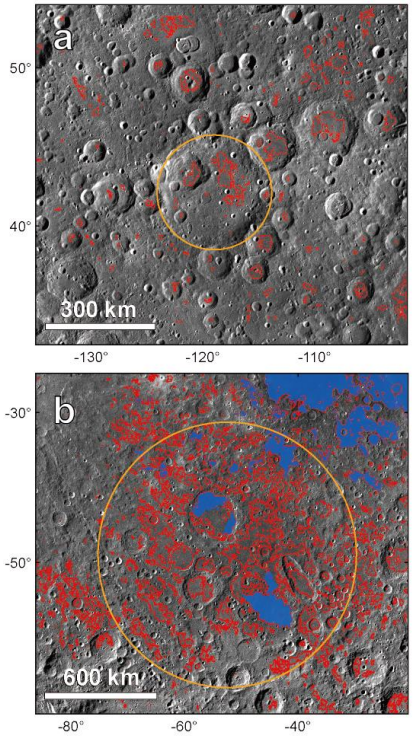

Fig. 2. Newly discovered melt and mare area (red boundaries). Blue area is the ground-truth mare basalt units from [6]. We infer (a) to be mainly impact melts, and (b) to be cryptomares. Yellow circles indicate the Landau crater and Schiller-Schickard crater. The locations of the two panels are shown in Fig. 1.

Acknowledgments: This work is supported by the Science and Technology Development Fund, Macau (0020/2021/A1) and NSFC 12173106.

References: [1] Head & Wilson (1992) *GCA, 56,* 2155–2175. [2] Laneuville et al. (2013) *JGR, 118,* 1435–1452. [3] Cintala et al. (1998) *M&PS, 33,* 889–912. [4] Neal et al. (2015) *GCA, 148,* 62–80. [5] Taguchi et al. (2017) *JGR, 122,* 1505–1521. [6] Nelson et al. (2014) *45th LPSC,* Abstract #2861. [7] Speyerer (2011) *42nd LPSC,* Abstract #2387. [8] Ronneberger et al. (2015) arXiv:1505.04597. [9] Kreslavsky et al. (2013) *Icarus, 226,* 52–66. [10] Whitten & Head (2015) *Icarus, 247,* 150–171. [11] Blewett (1995) *JGR, 100,* 16959–16977.